

# Ground and excited state properties of the polar and paramagnetic RbSr molecule: a comparative study.

Piotr S. Żuchowski,<sup>1,\*</sup> R. Guérout,<sup>2,†</sup> and O. Dulieu<sup>3,‡</sup>

<sup>1</sup>*Instytut Fizyki, Uniwersytet Mikołaja Kopernika, ul. Grudziadzka 5/7, 87-100 Toruń, Poland*

<sup>2</sup>*Laboratoire Kastler-Brossel, CNRS, ENS, UPMC, Case 74, F-75252 Paris, France*

<sup>3</sup>*Laboratoire Aimé Cotton, CNRS/ Univ. Paris-Sud/ ENS-Cachan,  
Bât. 505, Campus d'Orsay, 91405 Orsay Cedex, France.*

(Dated: February 5, 2014)

This paper deals with the electronic structure of RbSr, a molecule possessing both a permanent magnetic and electric dipole moment in its own frame allowing its manipulation with external fields. Two complementary *ab-initio* approaches are used for the ground and lowest excited states: first, an approach relying on optimized effective core potentials with core polarization potentials based on a full configuration interaction involving three valence electrons, and second, an approach using a small-size effective core potential with 19 correlated electrons in the framework of coupled-cluster theory. We have found excellent agreement between these two approaches for the ground state properties including the permanent dipole moment. We have focused on studies of excited states correlated to the two lowest asymptotes  $\text{Rb}(5p\ ^2P) + \text{Sr}(5s\ ^1S)$  and  $\text{Rb}(5s\ ^2S) + \text{Sr}(5s5p\ ^3P)$  relevant for ongoing experiments on quantum degenerate gases. We present also the Hund c) case potential curves obtained using atomic spin-orbit constants. These potential curves are an excellent starting point for experimental studies of molecular structure of RbSr using high-resolution spectroscopy.

PACS numbers: 34.20.-b, 34.50.Cx, 37.10.Pq

## I. INTRODUCTION

The detailed investigation of the properties of quantum degenerate gases of ultracold species (*i.e.* with kinetic energy  $E_k \equiv k_B T$  equivalent to a temperature  $T \ll 1$  millikelvin) is among the most important goals of modern atomic, molecular, optical and statistical physics. A unique feature of ultracold quantum gases is the tunability of the interaction strength between the particles with the external fields: by employing the Feshbach resonances [1] it is possible to change the scattering length in broad range of values. By comparison with atoms, the rich internal structure of polar molecules (*i.e.* possessing a permanent electric dipole moment) and their mutual strong anisotropic interactions can offer to this field novel opportunities for precision measurements and for quantum control using electromagnetic fields [2, 3]. Ultracold molecules trapped in periodic optical lattices have been proposed as qubits for prototypes of quantum computers [4], or as quantum simulators for studies of many-body phenomena such as phase transitions, strongly correlated systems or many-body physics in reduced dimensions [5, 6]. In 2008 two groups have reported the formation of ultracold gases of polar LiCs and KRb molecules in ultracold temperatures [7, 8]: ultracold LiCs molecules have been obtained by photoassociation of pairs of ultracold Li and Cs atoms and spontaneous decay of excited LiCs\* molecule down to the electronic ground state, while ultracold KRb molecules have

been created through magnetoassociation of ultracold K and Rb atoms into weakly bound levels of the molecular ground state, followed by stimulated Raman adiabatic passage (STIRAP) toward the lowest rovibrational level [9, 10]. There is also a number of other experiments aiming at creating ultracold heteronuclear diatomic alkali-metal molecules in their ground state like RbCs [11, 12] and NaK [13], since in contrast with KRb [14] they are stable with respect to the chemical reactions of atom exchange and trimer formation [15].

Heteronuclear diatomic alkali-metal molecules in their ground state  $X^1\Sigma^+$ , however, are not easy to manipulate with external fields: their very weak magnetic moment originates only from nuclear spin, and they do not exhibit a linear Stark effect in the rovibrational ground state. A very interesting class of quantum simulators has been proposed by Micheli *et al.* [5] employing molecules with both an electric and magnetic permanent dipole moment in their own frame. Such molecules reveal fascinating potential for high-precision measurements (for example the YbF molecule is being used in the determination of bounds for the electric dipole moment of the electron [16]) or for sensitive imaging of low-frequency electromagnetic fields [17]. In the rest of the paper we will qualify in short such species as paramagnetic and polar molecules.

One of the possible candidates for paramagnetic and polar molecules are diatomic molecules formed by association of laser-coolable atoms with different atomic spin quantum numbers, such as pairs of alkali-metal atoms and alkaline-earths atoms [18, 19]. One of the most promising candidates for such system is the RbSr molecule. Besides its magnetic doublet  $X^2\Sigma^+$  electronic ground state, it exhibits a permanent electric dipole moment of about 1.4-1.5 Debye [18, 19]. The laser cooling,

\* pzuch@fizyka.umk.pl

† romain.guerout@spectro.jussieu.fr

‡ olivier.dulieu@u-psud.fr

trapping and manipulation of Rb atoms have been well-established at the very beginning of the ultracold matter studies [20]. At present the strontium atom is one of the most popular atomic species in ultracold physics [21, 22]: for example, the studies of Bose-Einstein condensation of Sr atoms and Bose-Fermi mixtures (of different Sr isotopes) has recently been reported [23–27]. Moreover, the Innsbruck group has developed the STIRAP scheme to produce weakly bound  $\text{Sr}_2$  molecules in ground electronic state. It is finally worth mentioning that  $\text{Sr}_2$  molecules have also been produced by spontaneous decay from excited  $\text{Sr}(^1S)\text{--Sr}(^3P_1)$  molecular state [28]. More recently a quantum degenerate gas of rubidium atoms coexisting with strontium has been produced [29]. Another motivation which makes the studies of RbSr system particularly interesting is the magnetic tunability of scattering length due to presence of subtle mechanisms which can produce the Feshbach resonances [19]. That might allow the experimentalist to modify the scattering length in the ultracold mixture of Rb and Sr and control the behaviour of quantum gas of such atoms. It is worth mentioning that several other similar species are subject to intense ongoing research, like YbLi [30–34] and YbRb [35–37].

Manipulation of the quantum states of diatomic molecules with laser light requires the knowledge of appropriate transition energies, and thus of the potential energy curves (PECs) supporting the relevant energy levels and the corresponding transition dipole moments (TDMs). Surprisingly enough, still only little is known about the structure of molecules containing alkali-metal atoms with group II atoms. The electronic structure of Ba neutral compounds (BaLi, BaNa, BaK) has been explored some time ago by Allouche and coworkers [38–40]. Other studies concern CaLi [41–43], LiBe [44, 45]. More recently the electronic structure of the related molecular ions containing one alkali atom and  $\text{Ca}^+$  [46],  $\text{Sr}^+$  [47] or  $\text{Ba}^+$  [48–51] with various high-level approaches have been published in relation with experiments aiming at creating cold molecular ions in merged cold ion and cold atom traps.

In this paper we present the studies of interactions of Rb and Sr atoms in ground and excited states. We have recently examined this system in its  $X^2\Sigma^+$  ground state with two entirely different approaches [18, 19]: one relies on the representation of RbSr as a three-valence-electron molecule in the field of relativistic polarizable large effective core potentials (ECPs) through a full configuration interaction (FCI) calculation, while the other treats explicitly 19 electrons in the field of a relativistic small core ECP via the coupled cluster (CC) theory. Here, we use these approaches to revisit and to extend the study of the electronic structure of the RbSr system. The methods are described in Section II. The ground state properties of RbSr are carefully revisited in Section III including the potential curve, the permanent dipole moment, and the static dipole polarizability. We have calculated the PECs and the transition dipole moments between the  $X^2\Sigma^+$  ( $\text{Rb}(5s^2S)+\text{Sr}(5s^2^1S)$ ) ground state and the excited

$^2\Sigma^+$  and  $^2\Pi^+$  states correlated to the two lowest asymptotes  $\text{Rb}(5p^2P)+\text{Sr}(5s^2^1S)$  and  $\text{Rb}(5s^2S)+\text{Sr}(5s5p^3P)$  relevant for the ongoing experiments (Section IV). We have also investigated the spin-orbit (SO) coupling of these states within the framework of an atomic model involving experimental atomic SO splittings. The results of this paper are of key importance in experimental investigations of the spectroscopy and dynamics of the RbSr diatom. These data could be adjusted to spectroscopic data in order to provide the essential information for designing optical routes for the formation of ultracold ground-state RbSr molecules in their lowest internal level, thus opening the way toward a degenerate quantum gas of molecules with both magnetic and electric dipole moments. In the rest of the paper, atomic units for distances (1 a.u. =  $a_0=0.0529177$  nm), energies (1 a.u.= $2R_\infty=219474.63137$  cm $^{-1}$ ), and dipole moment (1 a.u.= $2.541\,580\,59$  Debye) will be used, except otherwise stated.

## II. METHODS

The first method is identical to the one used in our previous works for  $\text{RbSr}^+$  [47] and for the RbSr ground state [18]. It is based on the representation of the  $\text{Rb}^+$  and  $\text{Sr}^{2+}$  ionic cores by relativistic effective core potential (ECP) complemented with core polarization potential (CPP) simulating core-valence correlation along the lines developed by Müller and Meyer [52, 53] and Foucrault *et al.* [54]. These effective potentials involve semi-empirical parameters (reported in Ref.[18]) which are chosen to reproduce the energies of the lowest  $s$ ,  $p$  and  $d$  levels of the Rb and  $\text{Sr}^+$  one-valence-electron systems. A full configuration interaction method (FCI) involving three valence electrons is performed in the framework of the CIPSI method (Configuration Interaction by Perturbation of a multiconfiguration wave function Selected Iteratively) developed at Paul Sabatier University in Toulouse (France). From now on we will refer to this method as FCI/ECP+CPP. Previous works on alkali dimers (see for instance Refs.[55–57]) have demonstrated that this approach yields results for equilibrium distances ( $R_e$ ) and potential well depths ( $D_e$ ) for ground and excited states in good agreement with those obtained from experiments: for example, the discrepancy on  $D_e$  for the  $^1\Sigma^+$  ground states of alkali dimers is typically much less than 100cm $^{-1}$ , often (eg. for KRb) less than 20 cm $^{-1}$ . Values for permanent electric dipole moments (PEDMs) of their  $^1\Sigma^+$  ground state [55] match those measured in recent ultracold molecule experiments (*e.g.* for KRb [10], LiCs [58]). The TDMs functions are also found in close agreement with other theoretical values [56, 59, 60]. The (well-known) main advantage of the FCI/ECP+CPP method is its versatility and robustness: several low-lying excited states can be easily calculated regardless their total spin, in contrast to single-reference quantum chemistry methods we employ in this paper (see

below). Among disadvantages is its rapid increase of computational cost with increased basis set size. Just as in Ref.[18] the basis set used in these calculations was limited to  $s$ ,  $p$  and  $d$  Gaussian-type basis functions which translates into a number of configurations of about  $10^5$ . In the present case, the lack of  $f$  orbitals mostly affects the evaluation of the dispersion interaction *i.e.* its dependency in  $R^{-6}$  is well reproduced, but its magnitude may not be correct. The basis-set superposition error (BSSE) has not been introduced, as we have checked that it remains small (less than  $1 \text{ cm}^{-1}$ ) for the three valence electrons, while it is hard to estimate for the core electrons which are not explicitly taken in account.

The second method involves the calculations with fully relativistic small-core ECP (ECP28MDF) obtained by Lim *et al.* [61, 62], such that all  $4s$ ,  $4p$  and  $5s$  electrons (19) of Rb and Sr are correlated on both atoms. The PECs for the  $X^2\Sigma^+$  ground state and for the lowest quartet  $\Sigma^+$  and  $\Pi$  states are determined within the open-shell spin-restricted coupled-cluster (RCC) theory [63] with single, double and triple excitations (RCCSD(T)) as in Ref.19 implemented in the MOLPRO 2012 package [64]. In comparison to this work, we performed the calculations with significantly improved basis set in order to estimate the error attributed to the basis set incompleteness. We used the original uncontracted basis sets of Lim *et al.* [61, 62] to which we have added  $d$ ,  $f$  and  $g$  Gaussian-type basis functions to improve core-valence correlation between the  $4s$  and  $4p$  shells with the  $5s$  one. We also added a series of diffuse *spdfg* basis functions to better describe the dispersion interaction. We have further added  $3s3p3d2f2g$  bonding functions. We denote this new basis set with its maximum angular momentum  $l_{\text{max}} = 4$ . We have further extended this set to build a new one (denoted with  $l_{\text{max}} = 5$ ) including one more large-exponent  $g$  function for core-valence correlation and one diffuse  $h$  function. The latter has been used only for ground state calculations. Both basis sets are attached to this paper in the Supplementary material.

The doublet excited states have been obtained with the spin-restricted version of the open-shell equation-of-motion coupled cluster method limited to singly- and doubly- excited configurations (EOM-CCSD) [65, 66] implemented in the CFOUR package [67]. This approach allows for calculating excitation energies from the electronic ground state to the excited state of any spatial symmetry, but it is unable to calculate the spin-flip transitions (and thus those involving the quartet states). The excitation energies of doublet states obtained with EOM-CCSD method has been then added to the ground state potential energy curve, while the lowest  $1^4\Sigma^+$  and  $1^4\Pi$  PECs have been shifted in order to smoothly match the  $\text{Rb}(5s^2S) + \text{Sr}(5s5p^3P)$  asymptotes calculated with EOM-CCSD. The basis functions has been restricted to the  $l_{\text{max}} = 4$  set with removed bonding functions.

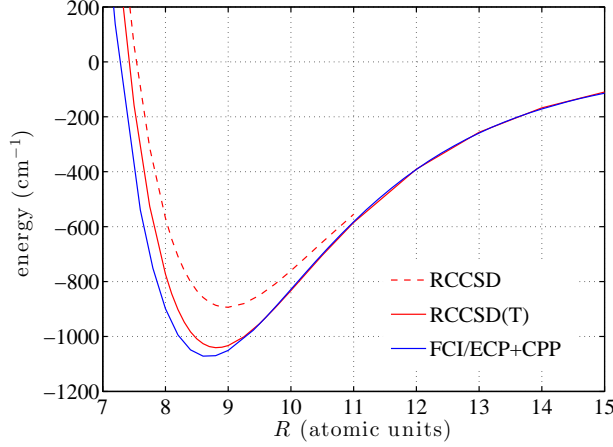
### III. THE GROUND STATE PROPERTIES OF RbSr

We present the results of our electronic-structure calculations for the ground state RbSr dimer using the RCCSD(T) method with both basis sets above in order to investigate the discrepancies between spectroscopic parameters obtained by Guérout *et al.* [18] and Żuchowski *et al.* [19], and to estimate the error bars due to the basis set truncation in CC calculations. Results are shown in Figure 1, while the essential spectroscopic parameters are gathered in Table I.

The ground state potential calculated with the FCI/ECP+CPP method [18] is  $D_e = 1073.3 \text{ cm}^{-1}$  deep with an equilibrium distance  $R_e = 8.69a_0$  while in Ref. 19 the depth of RbSr potential was found equal to  $1000 \text{ cm}^{-1}$  at  $R_e = 8.86a_0$ . With the new basis sets we have found that  $D_e$  is approximately 3-4% larger: the RCCSD(T) value is increased to  $D_e = 1034.4 \text{ cm}^{-1}$  with the  $l_{\text{max}} = 4$  basis set and to  $D_e = 1040.5 \text{ cm}^{-1}$  with the  $l_{\text{max}} = 5$  one. The difference in  $D_e$  in these basis sets is most likely related to a saturation of the dispersion energy in the calculations involving Gaussian functions. Based on well-know behavior of the correlation energy as a function of maximum angular momentum in the basis set [68] we can deduce the complete basis limit expected for RCCSD(T) method yielding a total interaction energy  $1047.9 \text{ cm}^{-1}$ . In fact, it is reasonable to treat the difference between extrapolated result and the interaction energy calculated using the  $l_{\text{max}} = 5$  basis set as the uncertainty of the calculation. It is still quite hard to estimate the error beyond the RCCSD(T) calculation and to this end we will compare how analogous methodology performs for the  $\text{Sr}_2$  and singlet  $\text{Rb}_2$  molecules. Skomorowski *et al.* have shown [69], that the CCSD(T) dissociation energy of the  $\text{Sr}_2$  dimer ( $1124 \text{ cm}^{-1}$ ), calculated with the same core potential and similar basis set, is slightly larger (by 3.8%) than the experimental dissociation energy ( $1082 \text{ cm}^{-1}$ ). The well depth of the  $\text{Rb}_2$  ground state CCSD(T) PEC obtained with the ECP and basis set used in present study underestimates the experimental value ( $3836 \text{ cm}^{-1}$ ) by 6%. Thus, taking a 5% uncertainty ( $52 \text{ cm}^{-1}$ ) on our basis set potential is certainly a conservative estimate. For completeness, we have also calculated the RbSr ground state PEC with spin-unrestricted coupled-cluster (UCC) approach: the potential depth for UCCSD(T) is no more than  $20 \text{ cm}^{-1}$  larger than in the restricted case, which is within the estimated error bound.

The result from the FCI/ECP+CPP calculation falls within such error bound, as the well depth is only  $33 \text{ cm}^{-1}$  deeper than the RCCSD(T) value. The agreement between harmonic constants  $\omega_e$  is also very good:  $38.98 \text{ cm}^{-1}$  with the FCI/ECP+CPP approach and  $38.09 \text{ cm}^{-1}$  with the RCCSD(T) calculations and the  $l_{\text{max}} = 5$  basis set. Note, however, that  $R_e$  is smaller by about  $0.1 a_0$  in the FCI/ECP+CPP approach than in the RCCSD(T). This is probably due to the short-range

FIG. 1. The RbSr ground state potential energy curves obtained with RCCSD (dashed red line), RCCSD(T) (full red line), and FCI/ECP+CPP methods (full blue line).



repulsion between the  $\text{Rb}^+$  and the  $\text{Sr}^{2+}$  cores which is not automatically included the FCI/ECP+CPP approach involving large cores. This contribution can be represented by an exponential expression [70, 71] fitted on the Hartree-Fock energy of the  $\text{RbSr}^{3+}$  system.

In fact both curves differ by merely one bound state and further two-color photoassociation spectroscopy for several isotopic mixtures of RbSr should provide the exact number of bound states supported by RbSr potential. The potential energy curves reported in this paper should be an excellent starting point for refinement using the experimental data.

Other properties of the RbSr ground-state reveal the present quality of the electronic wave function when results are compared between two methods. Figure 2 displays the ground state PEDM functions computed within the finite field approach, as obtained with the FCI/ECP+CPP method [18], and the new RCCSD(T) computation with extended basis set. Both approaches yield very similar variation and magnitude, and thus very similar electronic wave functions. At the equilibrium distance the PEDMs are almost identical (1.54 D), and they become slightly different only at short internuclear distances. Note, that with previously reported calculations [19] - with the RCCSD(T) method employing smaller basis set - the value of the dipole moment was found to be 1.36 D.

The similar finite-field approach allows for calculating the static dipole polarizability of the RbSr ground state as the second derivative of the RCCSD(T) energy with respect to the amplitude of an external electric field. We display in Fig. 3 the  $R$ -dependent isotropic polarizability  $\alpha_0$  and the corresponding anisotropy  $\Delta\alpha$  which are related to the cartesian components according to the

FIG. 2. Permanent electric dipole moment of RbSr ground state calculated with finite-field method through the RCCSD(T) (full blue line) and the FCI/ECP+CPP approach [18] (full red line).

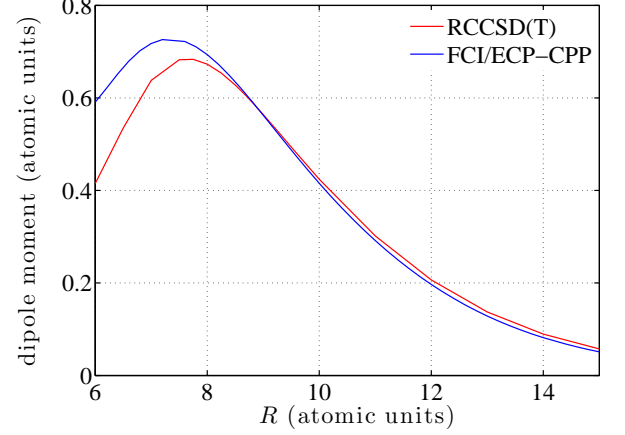
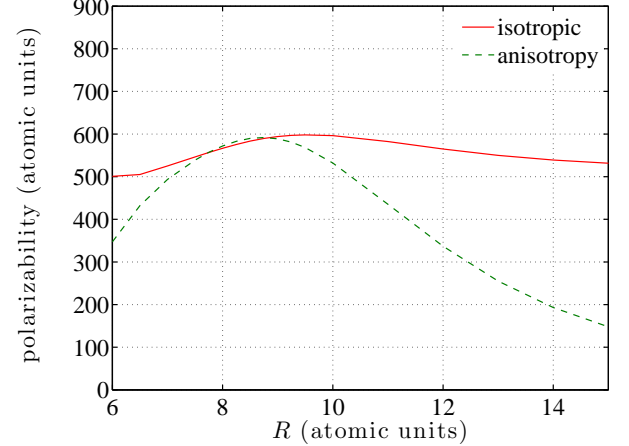


FIG. 3. Isotropic static dipole polarizability and the corresponding anisotropy of the RbSr ground state calculated with finite-field RCCSD(T) method.



well-known formula

$$\alpha_0 = \frac{1}{3}(2\alpha_{xx} + \alpha_{zz}) \quad \Delta\alpha = \alpha_{zz} - \alpha_{xx} \quad (1)$$

For the equilibrium distance the anisotropy of polarizability of RbSr molecule and the averaged polarizability are almost equal. The anisotropic polarizability peaks near  $R_e$  while  $\alpha_0$  has its maximum for  $9.6 a_0$ . The  $\Delta\alpha$  at equilibrium distance is very large and comparable to the largest anisotropies reported for alkali-metal dimers [7, 72]. With the large dipole moment and the large anisotropy of polarizability of RbSr, the RbSr molecule can be considered as a good candidate for manipulation with intense off-resonant laser light [73–75].



TABLE I. Equilibrium distance  $R_e$  (in  $a_0$ ) and potential depth  $D_e$  (in  $\text{cm}^{-1}$ ) of the RbSr ground state obtained by the various approaches discussed in the text.

method	$R_e(a_0)$	$D_e(\text{cm}^{-1})$
FCI/ECP+CPP, Ref. 18	8.69	1073.3
RCCSD(T), Ref. 19	8.86	999.6
$l_{\text{max}} = 4$ basis set		
RCCSD	8.99	885.6
RCCSD(T)	8.83	1034.4
UCCSD	8.99	898.5
UCCSD(T)	8.81	1052.5
$l_{\text{max}} = 5$ basis set		
RCCSD	8.98	893.6
RCCSD(T)	8.82	1040.5
UCCSD	8.97	896.7
UCCSD(T)	8.80	1059.1

#### IV. EXCITED STATES OF THE RbSr MOLECULE

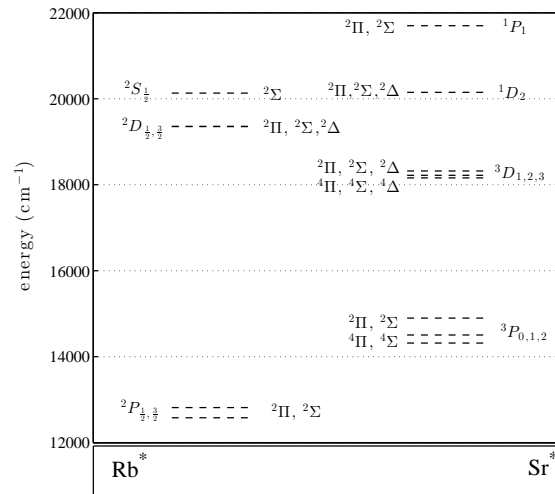
Figure 4 shows the diagram of the excited energy levels of Rb and Sr and lists the related Hund's (a) case states of RbSr. From the experimental point of view the most interesting excited states are those correlating with the lowest asymptotes  $\text{Rb}(^2S)+\text{Sr}(^3P_{0,1,2})$  and  $\text{Rb}(^2P)+\text{Sr}(^1S)$ . In particular the forbidden transition  $^1S \rightarrow ^3P_1$  in Sr atom is very appealing for photoassociation experiments and optical manipulation, due its narrow width. This intercombination line has also been used recently for creation of ground state  $\text{Sr}_2$  molecules [24, 28], and for optical tuning of the Sr scattering length [76–78]. We have also found that the states correlated to the  $\text{Rb}(^2S)+\text{Sr}(^3P)$  asymptote might interact with higher excited states, thus we have also explored few of them – namely the states which correlated to  $\text{Rb}(^2S)+\text{Sr}(^3D)$  and  $\text{Rb}(^2D)+\text{Sr}(^1S)$  asymptotes which are separated only by about  $1000 \text{ cm}^{-1}$ . Note that the  $\text{Rb}(6s^2S)$  and the  $\text{Sr}(5s4d^1D)$  levels are very close to each other ( $20132.5 \text{ cm}^{-1}$  and  $20149.7 \text{ cm}^{-1}$ ) so that the *ab-initio* calculations are very difficult to perform, regarding especially the proper order of asymptotic molecular states. The present approaches have been however successful in this matter.

The excited state PECs calculated with both methods presented in Section II are displayed in Figure 5, while in Table II we report the main spectroscopic parameters of the Hund's case (a) PECs correlated to  $\text{Rb}(^2S)+\text{Sr}(^3P_{0,1,2})$  and  $\text{Rb}(^2P)+\text{Sr}(^1S)$ .

##### A. The $\text{Rb}(5p^2P)-\text{Sr}(^1S)$ interaction

The two RbSr Hund's (a) case states correlated to this limit are denoted as  $2^2\Sigma^+$  and  $1^2\Pi$ . By construction

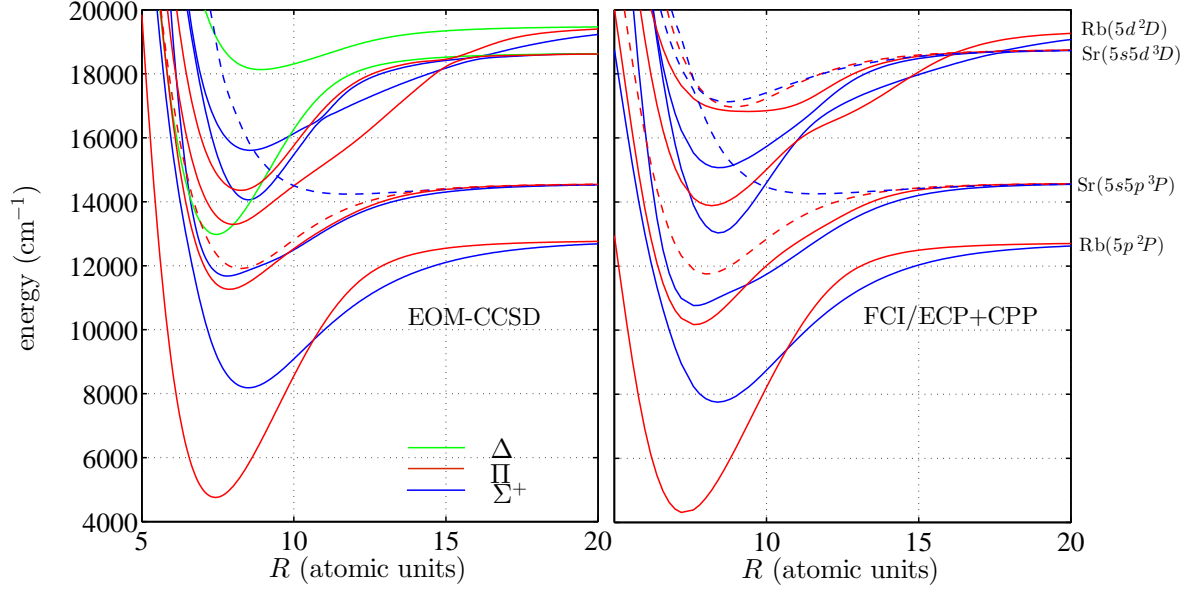
FIG. 4. The diagram of experimental excited energy levels of Rb and Sr atoms featuring the corresponding dissociation limits (adding a ground state Sr atom on the left column, and a ground state Rb atom on the right column) of the molecular Hund's (a) case states of the RbSr molecule. The Rb  $^2D_{3/2,5/2}$  energies of Rb are identical within the resolution of the plot. The origin of energies corresponds to infinitely separated ground state Sr and Rb atoms.



the FCI/ECP+CPP method involves the exact asymptotic energy of  $12737 \text{ cm}^{-1}$  (deduced from the position of  $P$ -state multiplet and Landé rule) while the EOM-CCSD method yields  $12793 \text{ cm}^{-1}$  in good agreement (better than 0.5%) with the former value. The overall agreement for the main spectroscopic quantities between FCI/ECP+CPP and EOM-CCSD PECs is satisfactory (see Table II). Just like for the ground state PEC, the FCI/ECP+CPP method gives equilibrium distances shorter by about  $0.1a_0$  compared to the EOM-CCSD ones. This is due to the modeling of the short-range core-core repulsion that can be assumed to be identical to the one used for the ground state. This feature is also partly responsible for the deeper well depth (by about 5-7%) and the smaller harmonic constant (by about 5%) obtained with the FCI/ECP+CPP method for both  $\Sigma$  and  $\Pi$  states compared to the EOM-CCSD results. Note that both methods place the crossing between the  $2^2\Sigma^+$  and  $1^2\Pi$  states at almost the same distance:  $10.67 a_0$  in case of the FCI/ECP+CPP and  $10.65 a_0$  for the EOM-CCSD method.

A very good agreement is found between the two methods on the PEDM of both the  $2^2\Sigma^+$  and  $1^2\Pi$  states (Fig. 6a) demonstrating again that both methods indeed describe the same electronic wave functions. The positions of maximum values of the PEDMs agree within  $0.1 a_0$ , whereas their (large) magnitudes at this point agree to better than 5%. The existence of two maxima in the  $2^2\Sigma^+$  PEDM is probably related to a sudden change of chemical character of RbSr molecule near

FIG. 5. Hund's case (a) potential energy curves of the excited RbSr molecule obtained with EOM-CCSD method (left panel) and FCI/ECP+CPP method (right panel).



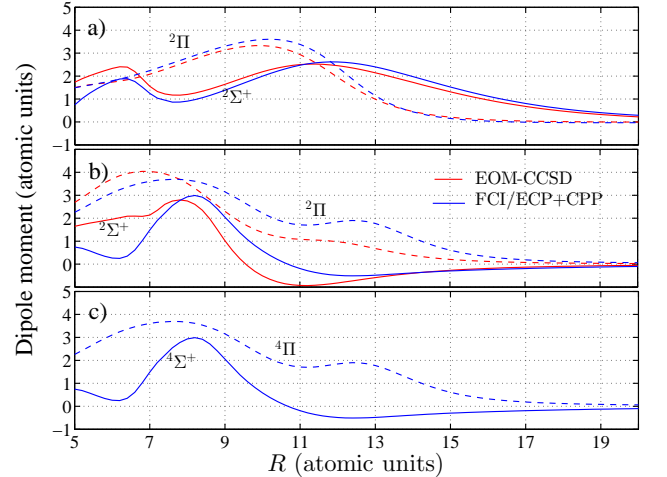
the repulsive wall into an ion-pair state. As can be expected from the previous results on PEDMs, the agreement on the TDM functions for these states (Fig. 7a) is also excellent between the two approaches, as they involve ground and excited state wave functions which are represented in almost identical ways. Note that the asymptotic limit of these TDMs (3.013 a.u.) calculated at very long range agrees very well with the experimental atomic value  $2S \rightarrow 2P_{1/2}$  transition (2.99 a.u.). At short distances the  $X^2\Sigma^+ \rightarrow 1^2\Pi$  transition is clearly favored with respect to the  $X^2\Sigma \rightarrow 2^2\Sigma$  transition.

### B. The Rb( $5s^2S$ )–Sr( $5s5p^3P$ ) interaction

Four Hund's case (a) molecular states are correlated to this asymptote, which are denoted as  $3^2\Sigma^+$ ,  $1^4\Sigma$ ,  $2^2\Pi$ , and  $1^4\Pi$ . All four states can easily be calculated with the FCI/ECP+CPP approach, while the computing codes for open-shell EOM-CCSD method for spin-changing states are not available. As mentioned in Section II, the  $1^4\Sigma^+$  and  $1^4\Pi$  quartet states correlating with Rb( $2S$ ) + Sr( $3P$ ) are the lowest ones for given spatial and spin symmetries, and are dominated by a single electronic configuration so that their PECs can be obtained with the RCCSD(T) method.

The asymptotic limit of obtained excitation energies for these states are correctly reproduced to better than 1% by our calculations when compared to the experimental value  $14705\text{ cm}^{-1}$  deduced from atomic data through

FIG. 6. Permanent electric dipole moments for (a) the  $2^2\Sigma^+$  and  $1^2\Pi$  states correlated to Rb( $5p^2P$ )–Sr( $5s^1S$ ), (b) the  $3^2\Sigma^+$  and  $2^2\Pi$  states correlated to Rb( $5s^2S$ ) + Sr( $5s5p^3P$ ), (c) the  $1^4\Sigma^+$  and  $1^4\Pi$  states correlated to Rb( $5s^2S$ ) + Sr( $5s5p^3P$ ), calculated with FCI/ECP+CPP and EOM-CCSD approaches. Solid lines:  $2,4\Sigma^+$  symmetry; dashed lines:  $2,4\Pi$  symmetry.

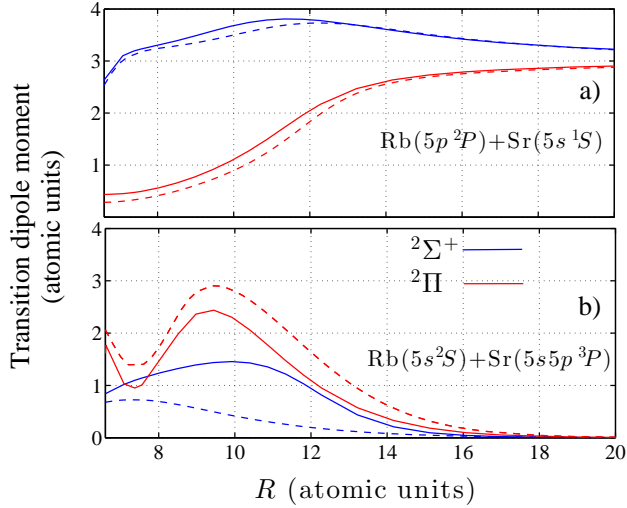


the Landé rule for the  $3P$  strontium multiplet. The FCI/ECP+CPP method yields  $14615\text{ cm}^{-1}$  [18] by construction for both the quartet and doublet states. The

TABLE II. Main spectroscopic parameters of the lowest excited states of RbSr Hund's case (a) potential energy curves

State	FCI/ECP+CPP			EOM-CC			asymptote
	$R_e (a_0)$	$D_e (\text{cm}^{-1})$	$\omega_e (\text{cm}^{-1})$	$R_e (a_0)$	$D_e (\text{cm}^{-1})$	$\omega_e (\text{cm}^{-1})$	
$1^2\Sigma^+$	8.69	1073.3	38.98	8.82	1040.5	38.09	$\text{Rb}(5s^2S)+\text{Sr}(^1S)$
$2^2\Sigma^+$	8.40	4982.9	58.37	8.51	4609.6	60.20	$\text{Rb}(5p^2P)+\text{Sr}(^1S)$
$3^2\Sigma^+$	7.67	3828.0	65.26	7.81	2892.4	62.48	$\text{Rb}(5s^2S)+\text{Sr}(5s5p^3P)$
$1^2\Pi$	7.31	8439.8	79.50	7.42	8038.6	83.19	$\text{Rb}(5p^2P)+\text{Sr}(^1S)$
$2^2\Pi$	7.65	4421.2	67.60	7.88	3303.5	63.37	$\text{Rb}(5s^2S)+\text{Sr}(5s5p^3P)$
$1^4\Sigma^+$	11.63	336.3	15.42	11.81	329.2	15.03*	$\text{Rb}(5s)+\text{Sr}(5s5p)$
$1^4\Pi$	8.06	2838.1	56.98	8.24	2655.7	54.95*	$\text{Rb}(5s)+\text{Sr}(5s5p)$

FIG. 7. Transition dipole moments from the RbSr ground state  $X^2\Sigma^+$  towards (a) the  $2^2\Sigma^+$  state (blue lines) and the  $1^2\Pi$  (red lines) state, (b) the  $3^2\Sigma^+$  state (blue lines) and the  $2^2\Pi$  (red lines) state, obtained with EOM-CC (full lines), and with FCI/ECP+CPP (dashed lines).



EOM-CCSD value for doublet states is  $14567.8 \text{ cm}^{-1}$ .

Being the lowest states of their symmetry, the main spectroscopic constants for the  $1^4\Sigma^+$  and  $1^4\Pi$  PECs show a good agreement between the two methods, similar to the one obtained for the ground state PEC (Table II). In contrast we immediately see from the Table and from Figure 5 that larger discrepancies are found between the two methods for doublet states. The equilibrium distance is now shorter by about  $0.2a_0$  in the FCI/ECP+CPP method, which could partly be accounted for the larger contribution of the core-core repulsion around  $7.6a_0$  than in the lowest states with a higher  $R_e$ . While consistent in magnitude, the harmonic constants differ by about  $4 \text{ cm}^{-1}$  between the two methods, which could be reduced if we account for the short-range core-core term. The largest discrepancy concerns the well depth of the  $3^2\Sigma^+$  and  $2^2\Pi$  states which is deeper by about  $1000 \text{ cm}^{-1}$  in the FCI/ECP+CPP results. The PEDM

functions of Figure 6b reveal that while having similar trends, the details of the electronic wave functions induce significant differences in the oscillating patterns, *i.e.* in the relative weights of the configurations. Obviously this feature transfers into the TDM functions of Figure 7b, in particular for the  $X^2\Sigma^+ \rightarrow 3^2\Sigma^+$  transition where the magnitude of the TDM is weaker by about a factor of 2 in the FCI/ECP+CPP results compared to the EOM-CC ones, probably related to the different position of the node visible in the  $3^2\Sigma^+$  PEDM. Nevertheless these TDMs deserve more attention. Asymptotically such transitions are in principle forbidden due to atomic spin-flip selection rule. Actually the  $^1S \rightarrow ^3P_1$  excitation is allowed by electric dipole transition due to second-order spin-orbit mixing with the higher  $^1P_1$  state, while the excitation towards the  $^3P_{0,2}$  states is strongly forbidden. In the molecular region, the disallowed transitions from ground state becomes allowed due to the Pauli exchange interaction which can be measured by the magnitude of the exchange energy [79]. The quite sudden increase of the TDM around  $15a_0$  reflects the exponential variation of this exchange energy when the valence-overlap region is reached.

Further studies with EOM-CC method which includes triply excited clusters and all-electron relativistic studies could probably help to validate one of these results. Note that in the FCI/ECP+CPP approach the  $1^4\Pi$  state is well separated in energy from other states to which it is coupled by spin-orbit interaction (see next Section), while it crosses the doublet states in the EOM-CC method. If the former result would be confirmed, this means that strongly polar metastable RbSr molecules could be created and used for further manipulation in the experiments.

### C. Higher excited states

Higher excited states of RbSr cannot be disregarded from the present analysis. An inspection of Figure 5 shows that the  $3^2\Pi$  and  $4^2\Sigma^+$  PECs correlated to the  $\text{Rb}(5s^2S)+\text{Sr}(5s4d^3D)$  dissociation limit are submerged below the  $\text{Rb}(5s^2S)+\text{Sr}(5s5p^3P)$  asymptote by several

hundreds of  $\text{cm}^{-1}$  in both methods. The bottom of the well of the  $1^2\Delta$  state (computed with the EOM-CCSD approach) is submerged by more than  $1000 \text{ cm}^{-1}$  below that asymptote. Moreover, due to the proximity of their asymptotes, the excited states which correlate with  $\text{Rb}(4d^2D)+\text{Sr}(5s^2^1S)$ ,  $\text{Rb}(5s^2S)+\text{Sr}(5s4d^3D)$ , and  $\text{Rb}(5s^2S)+\text{Sr}(5s4d^1D)$  strongly mix together and exhibit numerous avoided crossings which are consistently predicted by both methods: around  $16a_0$  for the  $^2\Pi$  states, and around  $16a_0$  (EOM-CCSD) or  $18a_0$  (FCI/ECP+CPP) for the  $^2\Sigma^+$  states. Both approaches also predict the presence of short-range avoided crossings of  $\Pi$  and  $\Sigma^+$  states but with more pronounced differences in positions. Finally, we observe the large difference in the potential wells depths for  $\Pi$  and  $\Sigma^+$  states correlated to  $\text{Rb}(4d^2D)+\text{Sr}(5s^2^1S)$  and  $\text{Rb}(5s^2S)+\text{Sr}(5s4d^3D)$ .

#### D. Long-range behavior close to the $\text{Rb}(5p^2P)+\text{Sr}(5s^2^1S)$ and $\text{Rb}(5s^2S)+\text{Sr}(5s5p^3P)$ asymptotes

We have obtained the  $C_6$  values for the excited states by fitting the calculated potential energy curves at long range to  $C_6R^{-6}$  analytic form. This procedure has to be performed very carefully: backing out the van der Waals coefficients from the potential curves needs very high precision potential curves for broad range of distances. As invoked in Section II due to the lack of high angular momentum functions in the basis set used in the FCI/ECP+CPP computations, we performed such fittings only for the CC methods. For the doublet states correlated to the  $\text{Rb}(5p^2P)+\text{Sr}(5s^2^1S)$  limit we obtained  $C_6(2^2\Sigma^+) = 23324 E_h a_0^6$  and  $C_6(1^2\Pi) = 8436 E_h a_0^6$  compared to the values of Ref.[80],  $17530 E_h a_0^6$  and  $8331 E_h a_0^6$ , respectively. Despite the nice agreement obtained for the latter value, error bars for these values can be large and unpredictable as these values were obtained by fitting to the shape of EOM-CCSD potential curve added to the ground state interaction energy of RbSr. In contrast, the  $C_6$  values for the excited states correlating with  $\text{Rb}(5s^2S)+\text{Sr}(5s5p^3P)$  can be extracted with much better accuracy, since for the quartet states potential en-

ergy curves are obtained in direct way and not as a sum of interaction energy + EOM-CC excitation. We obtained  $C_6(2^2\Sigma^+) = 5265 E_h a_0^6$  and  $C_6(1^2\Pi) = 4654 E_h a_0^6$  which are in satisfactory agreement with the values  $5735 E_h a_0^6$  and  $5000 E_h a_0^6$  of Ref.[80].

#### E. Relativistic picture of the lowest excited states of RbSr.

Spin-orbit (SO) splittings are quite large for the lowest excited states of both atoms:  $237.6 \text{ cm}^{-1}$  for  $\text{Rb}(5p^2P)$  and  $581.1 \text{ cm}^{-1}$  for  $\text{Sr}(5s5p^3P)$ . Therefore they must be taken in account in any accurate representation of the RbSr excited states for the purpose of modelling experimental results. It is well-known that due to configuration mixing the SO couplings vary with the internuclear distance and can be reduced or enhanced typically by 30-50% compared to the atomic values. Examples can be found for instance in spectroscopic studies of RbCs [81], KCs [60], or in quantum chemistry studies of  $\text{Sr}_2$  [82],  $\text{SrYb}$  [83] or  $\text{Rb}_2$  [84]. It is beyond the goal of this paper to compute the  $R$ -dependence of the SO coupling in RbSr. Instead we present an approximate model where the atomic SO is used as a perturbation to the Hund's case (a) states, in order to deliver a preliminary picture of the relevant PECs. Due to the large energy separation of the  $\text{Rb}(5p^2P)+\text{Sr}(^1S)$  and  $\text{Rb}(5s^2S)+\text{Sr}(5s5p^3P)$  asymptotes, the corresponding manifold of PECs can safely be considered as isolated from each other. We will also ignore the higher excited states discussed above which are submerged below the  $\text{Rb}(5s^2S)+\text{Sr}(5s5p^3P)$  asymptote.

We follow the usual spectroscopic convention and use symbols  $\Lambda$ ,  $\Sigma$  for the projection onto the molecular axis of the electronic quantities namely the orbital angular momentum and the spin, respectively, and  $\Omega = |\Lambda + \Sigma|$ . The atomic SO constants are  $A_{\text{Rb}} = \Delta E_{\text{fs}}(\text{Rb}(5p^2P))/3 = 79.2 \text{ cm}^{-1}$  and  $A_{\text{Sr}} = \Delta E_{\text{fs}}(\text{Sr}(5s5p^3P))/3 = 193.7 \text{ cm}^{-1}$ . We use the fact that the matrix elements of spin-orbit Hamiltonian  $H_{\text{SO}} = \mathbf{A}\mathbf{L} \cdot \mathbf{S}$  in the basis  $|SL\Sigma\Lambda\rangle$  can be expressed in the *asymptotic* basis set of atomic angular momenta using Clebsch-Gordon coefficients:

$$|SL\Sigma\Lambda\rangle = \sum_{\Sigma_{\text{Rb}}, \Sigma_{\text{Sr}}} \langle S_{\text{Rb}}\Sigma_{\text{Rb}} S_{\text{Sr}}\Sigma_{\text{Sr}} | S\Sigma \rangle |S_{\text{Rb}}\Sigma_{\text{Rb}}\rangle |S_{\text{Sr}}L\Sigma_{\text{Sr}}\Lambda\rangle, \quad (2)$$

which more specifically reduces for doublet states to

$$|\frac{1}{2}L \pm \frac{1}{2}\Lambda\rangle = \pm \sqrt{\frac{1}{3}} |\frac{1}{2}\frac{1}{2}\rangle_{\text{Rb}} |1L0\Lambda\rangle_{\text{Sr}} \mp \sqrt{\frac{2}{3}} |\frac{1}{2} - \frac{1}{2}\rangle_{\text{Rb}} |1L1\Lambda\rangle_{\text{Sr}}, \quad (3)$$

while for the quartet states it reads

$$|\frac{3}{2}L \pm \frac{1}{2}\Lambda\rangle = \sqrt{\frac{1}{3}} |\frac{1}{2}\frac{1}{2}\rangle_{\text{Rb}} |1L0\Lambda\rangle_{\text{Sr}} + \sqrt{\frac{2}{3}} |\frac{1}{2} - \frac{1}{2}\rangle_{\text{Rb}} |1L1\Lambda\rangle_{\text{Sr}}, \quad (4)$$

$$|\frac{3}{2}L \pm \frac{3}{2}\Lambda\rangle = |\frac{1}{2} \pm \frac{1}{2}\rangle_{\text{Rb}} |1L \pm 1\Lambda\rangle_{\text{Sr}}. \quad (5)$$



The interaction of rubidium atom in the  $^2P$  state with Sr ground state atom splits the degeneracy of the  $^2P$  state into  $^2\Sigma$  and  $^2\Pi$  state. The total angular momentum projection  $|\Omega|$  can then take the values  $\frac{1}{2}$  and  $\frac{3}{2}$ . A unique state  $|\Omega| = \frac{3}{2}$  originates from  $^2\Pi(\Sigma = \pm\frac{1}{2}, \pm\Lambda = 1)$  state, while two states with  $|\Omega| = \frac{1}{2}$  states originate from mixing of the  $^2\Pi(\Sigma = \pm\frac{1}{2}, \Lambda = \mp 1)$  and  $^2\Sigma^+(\Sigma = \pm\frac{1}{2}, \Lambda = 0)$ . The Hamiltonian for the  $|\Omega| = \frac{3}{2}$  state is trivially reduced to one element only, which can be written as  $H(|\Omega| = \frac{3}{2}) = V(^2\Pi) + 2A_{\text{Rb}}$  and asymptotically corresponds to  $j = \frac{3}{2}$  state of the Rb atom. For the  $|\Omega| = \frac{1}{2}$  state the Hamiltonian can be written as

---


$$H(|\Omega| = \frac{1}{2}) = \begin{pmatrix} V(^2\Sigma) & \sqrt{2}A_{\text{Rb}} \\ \sqrt{2}A_{\text{Rb}} & V(^1^2\Pi) + A_{\text{Rb}} \end{pmatrix}. \quad (6)$$


---

Two of these states asymptotically correspond to the  $^3P_2$  Sr state, and one to the  $^3P_1$  Sr state. Finally, for the  $|\Omega| = \frac{1}{2}$  we have five states involved:  $^2\Sigma^+(\Sigma = \pm\frac{1}{2}, \Lambda = 0)$ ,  $^2\Pi(\Sigma = \mp\frac{1}{2}, \Lambda = \pm 1)$ ,  $^4\Sigma^+(\Sigma = \pm\frac{1}{2}, \Lambda = 0)$ ,

---

$$H(|\Omega| = \frac{3}{2}) = \begin{pmatrix} V(^2\Pi) + \frac{2}{3}A_{\text{Sr}} & \sqrt{\frac{1}{3}}A_{\text{Sr}} & -\frac{\sqrt{2}}{3}A_{\text{Sr}} \\ \sqrt{\frac{1}{3}}A_{\text{Sr}} & V(^4\Sigma) & \sqrt{\frac{2}{3}}A_{\text{Sr}} \\ -\frac{\sqrt{2}}{3}A_{\text{Sr}} & \sqrt{\frac{2}{3}}A_{\text{Sr}} & V(^4\Pi) + \frac{1}{3}A_{\text{Sr}} \end{pmatrix}. \quad (7)$$


---

Two eigenvalues of this matrix asymptotically correspond to both  $j = \frac{1}{2}, \frac{3}{2}$ , state of excited Rb( $5p$ ) atom.

For the interaction of  $^3P$  state of Sr and  $^2S$  of Rb the situation is somewhat more complicated. As we have mentioned in previous sections, the resulting dimer states for the Rb( $5s^2S$ )-Sr( $5s5p^3P$ ) interaction in the Hund's case (a) are  $^{2,4}\Sigma^+$  and  $^{2,4}\Pi$ . The possible quantum numbers for spin-orbit coupled states for that case are  $|\Omega| = \frac{1}{2}, \frac{3}{2}$  and  $\frac{5}{2}$ . The maximal value of  $|\Omega|$  corresponds trivially to single state, namely  $H(|\Omega| = \frac{5}{2}) = V(^1^4\Pi) + A_{\text{Sr}}$  asymptotically corresponding to the metastable state of Sr atom  $^3P_2$ . The  $|\Omega| = \frac{3}{2}$  states can be obtained by coupling of three states:  $^4\Sigma^+(\Sigma = \pm\frac{3}{2}, \Lambda = 0)$ ,  $^2\Pi(\Sigma = \pm\frac{1}{2}, \Lambda = \pm 1)$  and  $^4\Pi(\Sigma = \pm\frac{1}{2}, \Lambda = \pm 1)$ . The corresponding Hamiltonian from which we can obtain the Hund (c) case representation reads:

$^4\Pi(\Sigma = \mp\frac{1}{2}, \Lambda = \pm 1)$ ,  $^4\Pi(\Sigma = \pm\frac{3}{2}, \Lambda = \mp 1)$ . The Hamiltonian which describes the coupled  $|\Omega| = \frac{1}{2}$  states has the following form:

---

$$H(|\Omega| = \frac{1}{2}) = \begin{pmatrix} V(^2\Sigma^+) & \sqrt{\frac{8}{9}}A_{\text{Sr}} & 0 & -\frac{1}{3}A_{\text{Sr}} & \sqrt{\frac{1}{3}}A_{\text{Sr}} \\ \sqrt{\frac{8}{9}}A_{\text{Sr}} & V(^2\Pi) - \frac{2}{3}A_{\text{Sr}} & \frac{1}{3}A_{\text{Sr}} & -\frac{\sqrt{2}}{3}A_{\text{Sr}} & 0 \\ 0 & \frac{1}{3}A_{\text{Sr}} & V(^4\Sigma^+) & \sqrt{\frac{8}{9}}A_{\text{Sr}} & \sqrt{\frac{2}{3}}A_{\text{Sr}} \\ -\frac{1}{3}A_{\text{Sr}} & -\frac{\sqrt{2}}{3}A_{\text{Sr}} & \sqrt{\frac{8}{9}}A_{\text{Sr}} & V(^4\Pi) - \frac{1}{3}A_{\text{Sr}} & 0 \\ \sqrt{\frac{1}{3}}A_{\text{Sr}} & 0 & \sqrt{\frac{2}{3}}A_{\text{Sr}} & 0 & V(^4\Pi) - A_{\text{Sr}} \end{pmatrix}. \quad (8)$$

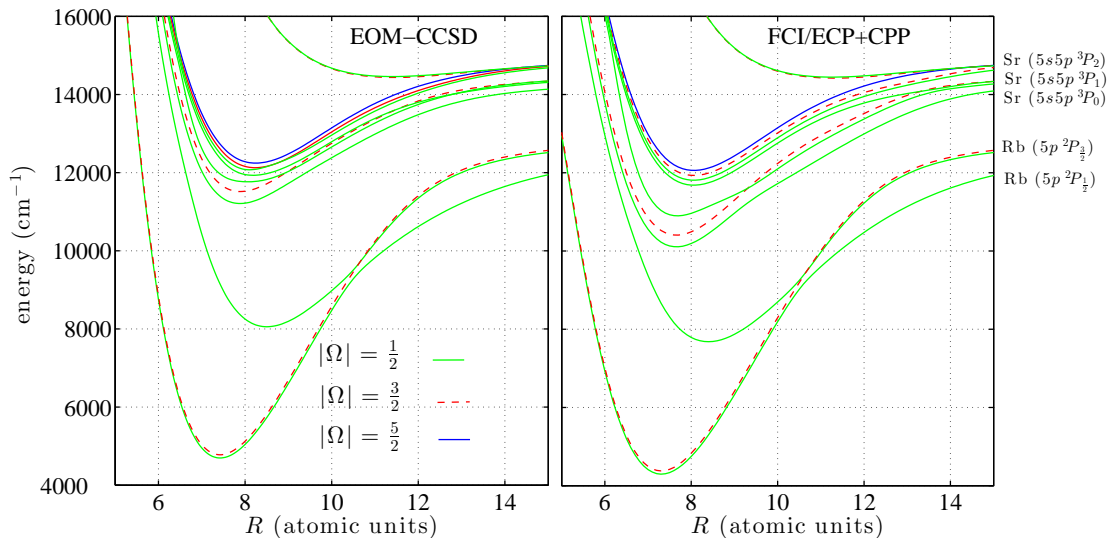

---

The eigenstates of the Hamiltonian for  $\Omega = \frac{1}{2}$  correspond to all components of the  $^3P$  asymptote of the excited Sr atom: the lowest eigenvalue represents the interaction of Rb atom with  $^3P_0$  state of Sr, two states correspond to the interaction with  $^3P_1$ , and two with  $^3P_2$ . The resulting spin-orbit coupled PECs are shown in Figure 8. The EOM-CC and FCI/ECP+CPP approaches give a very consistent potential energy curves, except some of the states which correlate with the Rb( $5s^2S$ )+Sr( $5s5p^3P_{0,1,2}$ ) asymptote, which originate from doublet  $3^2\Sigma^+$  and  $2^2\Pi$  states which are about 20% deeper in case of the FCI/ECP+CPP method.

For the Rb( $5p^2P_{1/2,3/2}$ )-Sr( $1S$ ) manifold the  $|\Omega| = \frac{1}{2}$  curves exhibit the avoided crossing in place where the

$1^2\Pi$  and  $2^2\Sigma^+$  states cross. Since the  $1^2\Pi$  and  $2^2\Sigma^+$  states are separated in energy by a much larger amount than the SO constant  $A_{\text{Rb}}$ , they preserve their Hund (a) case character over most of the internuclear distances in the chemical range. However the corresponding bound levels may well be strongly coupled as it is the case for instance in the heavy alkali-metal dimers like Rb<sub>2</sub> [85]. For the states that correlate with the Rb( $5s^2S$ )+Sr( $5s5p^3P_{0,1,2}$ ) asymptote the character of Hund's case (c) states is drastically changed, since the  $2^2\Pi$  and  $3^2\Sigma^+$ , and also  $1^4\Pi$  states are much closer in energy. Therefore these states are strong mixtures of doublet and quartet states. It is also clear from Figure 8 that among the states which correlate with

FIG. 8. EOM-CCSD potential energy curves of RbSr excited states including atomic spin-orbit interaction as explained in the text. (a) EOM-CC approach, (b) FCI/ECP+CPP approach.



Rb( $5s^2S$ )+Sr( $5s5p^3P_2$ ) there are states with  $|\Omega| = \frac{1}{2}$  and  $|\Omega| = \frac{3}{2}$  of very strong  $^4\Sigma^+$  character. Also, in view of such strong mixing, it is clear that the state  $|\Omega| = \frac{1}{2}$  which correlates with Sr atomic clock line will have nonzero transition dipole moment at finite distances. Hence, the vibrational states supported by such state might be accessible with dipole transitions.

## V. CONCLUSIONS AND OUTLOOK

In this work we have explored the ground and excited states of the RbSr molecule, which is a good candidate paramagnetic, polar molecule and subject to intense experimental study. A primary goal of this paper was to provide the first calculation of potential energy curves for the RbSr curves and dipole moment matrix elements and comparison between two *ab-initio* methods: FCI method with the use of ECP and CPP, and CC theory based methods used with small effective core potential.

It is usually difficult to provide error bound for the *ab-initio* calculations, unless we deal with small, few-electron system [86], for which it is possible to study the convergence pattern not only for systematically increased gaussian basis set but also for number of excitations introduced to the electronic wavefunction. Hence, for such complicated system as RbSr molecule application of two different methods provides a better starting point for further modelling of potential curves with help of high-resolution spectroscopy experiments. The discrepancies in calculations of potential energy curves between the methods used in this paper are very small for the ground state, for the states correlating with Rb asymptotes and for the quartet states correlating with the stron-

tium asymptotes. A bit larger discrepancies have been obtained for the doublet states of Rb+Sr( $5p$ ) systems, although the equilibrium distances and harmonic constants are consistent. For the higher excited states the agreement is moderately good.

Using both methods we have found that a very good agreement of the values of permanent dipole moments of the ground state RbSr system as well as doublet Rb( $5p$ )+Sr and Rb+Sr( $5p$ ) states: interestingly enough, the permanent dipole moments of the excited states are very large.

Finally, we have obtained the transition dipole moments for the excitations from the ground electronic state to Rb( $5p$ )+Sr and Rb+Sr( $5p$ ) states. Again, there is a good agreement between the two approaches used in this paper. Interestingly enough we have found that there are non-zero transition dipole moments from the ground state to doublet Rb+Sr( $5p$ ). That means, the possibility of driving for the dipole transitions to the vibrational states supported by the electronic states that correlate with strongly forbidden  $^3P_J$  lines of the strontium atom.

## VI. ACKNOWLEDGEMENTS

This work was supported in part by the National Science Foundation (Grant No. NSF PHY11-25915). RG acknowledges support from the *Institut Francilien de Recherches sur les Atomes Froids*. PSZ is grateful for the support of the Foundation for Polish Science Homing Plus Programme (2011 3/14) co-financed by the European Regional Development Fund. The authors are also grateful to Florian Schreck and Benjamin Pasquiou for sparking their interest in the RbSr system.

- 
- [1] C. Chin, R. Grimm, P. Julienne, and E. Tiesinga, *Rev. Mod. Phys.* **82**, 1225 (2010).
- [2] L. D. Carr and J. Ye, *New J. Phys.* **11**, 055009 (2009).
- [3] O. Dulieu and C. Gabbanini, *Rep. Prog. Phys.* **72**, 086401 (2009).
- [4] D. DeMille, *Phys. Rev. Lett.* **88**, 067901 (2002).
- [5] A. Micheli, G. K. Brennen, and P. Zoller, *Nature Physics* **2**, 341 (2006).
- [6] I. Bloch, J. Dalibard, and W. Zwerger, *Rev. Mod. Phys.* **80**, 885 (2008).
- [7] J. Deiglmayr, A. Grochola, M. Repp, K. Mörtlbauer, C. Glück, J. Lange, O. Dulieu, R. Wester, and M. Weidemüller, *Phys. Rev. Lett.* **101**, 133004 (2008).
- [8] K.-K. Ni, S. Ospelkaus, M. H. G. de Miranda, A. Pe'er, B. Neyenhuis, J. J. Zirbel, S. Kotochigova, P. S. Julienne, D. S. Jin, and J. Ye, *Science* **322**, 231 (2008).
- [9] S. Ospelkaus, A. Pe'er, K.-K. Ni, J. J. Zirbel, B. Neyenhuis, S. Kotochigova, P. S. Julienne, J. Ye, and D. S. Jin, *Nature Physics* **4**, 622 (2008).
- [10] K.-K. Ni, S. Ospelkaus, M. H. G. de Miranda, A. Peer, B. Neyenhuis, J. J. Zirbel, S. Kotochigova, P. S. Julienne, D. S. Jin, and J. Ye, *Science* **322**, 231 (2008).
- [11] M. Debatin, T. Takekoshi, R. Rameshan, L. Reichsoellner, F. Ferlaino, R. Grimm, R. Vexiau, N. Bouloufa, O. Dulieu, and H.-C. Naegerl, *Phys. Chem. Chem. Phys.* **13**, 18926 (2011).
- [12] T. Takekoshi, M. Debatin, R. Rameshan, F. Ferlaino, R. Grimm, H.-C. Nägerl, C. R. Le Sueur, J. M. Hutson, P. S. Julienne, S. Kotochigova, and E. Tiemann, *Phys. Rev. A* **85**, 032506 (2012).
- [13] C.-H. Wu, J. W. Park, P. Ahmadi, S. Will, and M. W. Zwiernik, *Phys. Rev. Lett.* **109**, 085301 (2012).
- [14] S. Ospelkaus, K.-K. Ni, D. Wang, M. H. G. de Miranda, B. Neyenhuis, G. Quémener, P. S. Julienne, J. L. Bohn, D. S. Jin, and J. Ye, *Science* **327**, 853 (2010).
- [15] P. S. Żuchowski and J. M. Hutson, *Phys. Rev. A* **82**, 060703 (2010).
- [16] J. J. Hudson, B. E. Sauer, M. R. Tarbutt, and E. A. Hinds, *Phys. Rev. Lett.* **89**, 023003 (2002).
- [17] S. V. Alyabyshev, M. Lemeshko, and R. V. Krems, *Phys. Rev. A* **86**, 013409 (2012).
- [18] R. Guérout, M. Aymar, and O. Dulieu, *Phys. Rev. A* **82**, 042508 (2010).
- [19] P. S. Żuchowski, J. Aldegunde, and J. M. Hutson, *Phys. Rev. Lett.* **105**, 153201 (2010).
- [20] M. H. Anderson, J. R. Ensher, M. R. Matthews, C. E. Wieman, and E. A. Cornell, *Science* **269**, 198 (1995).
- [21] P. G. Mickelson, Y. N. Martinez, A. D. Saenz, S. B. Nagel, Y. C. Chen, T. C. Killian, P. Pellegrini, and R. Cote, *Phys. Rev. Lett.* **95**, 223002 (2005).
- [22] S. B. Nagel, P. G. Mickelson, A. D. Saenz, Y. N. Martinez, Y. C. Chen, T. C. Killian, P. Pellegrini, and R. Côté, *Phys. Rev. Lett.* **94**, 083004 (2005).
- [23] S. Stellmer, M. K. Tey, B. Huang, R. Grimm, and F. Schreck, *Phys. Rev. Lett.* **103**, 200401 (2009).
- [24] S. Stellmer, B. Pasquiou, R. Grimm, and F. Schreck, *Phys. Rev. Lett.* **109**, 115302 (2012).
- [25] S. Stellmer, R. Grimm, and F. Schreck, *Phys. Rev. A* **87**, 013611 (2013).
- [26] S. Stellmer, M. K. Tey, R. Grimm, and F. Schreck, *Phys. Rev. A* **82**, 041602 (2010).
- [27] M. K. Tey, S. Stellmer, R. Grimm, and F. Schreck, *Phys. Rev. A* **82**, 011608 (2010).
- [28] G. Reinaudi, C. B. Osborn, M. McDonald, S. Kotochigova, and T. Zelevinsky, *Phys. Rev. Lett.* **109**, 115303 (2012).
- [29] B. Pasquiou, A. Bayerle, S. M. Tzanova, S. Stellmer, J. Szczepkowski, M. Parigger, R. Grimm, and F. Schreck, *Phys. Rev. A* **88**, 023601 (2013).
- [30] M. Okano, H. Hara, M. Muramatsu, K. Doi, S. Uetake, Y. Takasu, and Y. Takahashi, *Applied Physics B: Lasers and Optics* **98**, 691 (2010), 10.1007/s00340-009-3728-0.
- [31] H. Hara, Y. Takasu, Y. Yamaoka, J. M. Doyle, and Y. Takahashi, *Phys. Rev. Lett.* **106**, 205304 (2011).
- [32] A. H. Hansen, A. Khramov, W. H. Dowd, A. O. Jamison, V. V. Ivanov, and S. Gupta, *Phys. Rev. A* **84**, 011606 (2011).
- [33] P. Zhang, H. R. Sadeghpour, and A. Dalgarno, *J. Chem. Phys.* **133**, 044306 (2010).
- [34] G. Gopakumar, M. Abe, B. P. Das, M. Hada, and K. Hirao, *J. Chem. Phys.* **133**, 124317 (2010).
- [35] L. K. Sørensen, S. Knecht, T. Fleig, and C. M. Marian, *J. Phys. Chem. A* **113**, 12607 (2009).
- [36] N. Nemitz, F. Baumer, F. Münchow, S. Tassy, and A. Görlitz, *Phys. Rev. A* **79**, 061403 (2009).
- [37] M. Borkowski, P. S. Żuchowski, R. Ciurylo, P. S. Julienne, D. Kedziera, L. Mentel, P. Tecmer, F. Münchow, C. Bruni, and A. Görlitz, "Scattering lengths in isotopologues of the rbyb system," (2013), arXiv:1309.3131.
- [38] A. R. Allouche and M. Aubert-Frécon, *J. Chem. Phys.* **100**, 938 (1994).
- [39] N. Boutassetta, A. R. Allouche, and M. Aubert-Frécon, *Chem. Phys.* **189**, 33 (1994).
- [40] N. Boutassetta, A. R. Allouche, and M. Aubert-Frécon, *Chem. Phys.* **189**, 393 (1995).
- [41] A. R. Allouche and M. Aubert-Frécon, *Chem. Phys. Lett.* **222**, 524 (1994).
- [42] L. M. Russon, G. K. Rothschof, M. D. Morse, A. I. Boldyrev, and J. Simons, *J. Chem. Phys.* **109**, 6655 (1998).
- [43] M. Ivanova, A. Stein, A. Pashov, A. V. Stoloyarov, H. Knöckel, and E. Tiemann, *J. Chem. Phys.* **135**, 174303 (2011).
- [44] K. Pak, W. C. Ermler, C. W. Kern, and V. E. Bondybey, *J. Cluster Science* **2**, 19 (1991).
- [45] M. M. Marino, W. C. Ermler, C. W. Kern, and V. E. Bondybey, *J. Chem. Phys.* **96**, 3756 (1992).
- [46] F. H. Hall, P. Eberle, G. Hegi, M. Raoult, M. Aymar, O. Dulieu, and S. Willitsch, *Molecular Physics* **111**, 2020 (2013).
- [47] M. Aymar, R. Guérout, and O. Dulieu, *J. Chem. Phys.* **135**, 064305 (2011).
- [48] S. Knecht, H. J. A. Jensen, and T. Fleig, *J. Chem. Phys.* **128**, 014108 (2008).
- [49] S. Knecht, L. K. Sørensen, H. J. A. Jensen, T. Fleig, and C. M. Marian, *J. Phys. B* **43**, 055101 (2010).
- [50] M. Krych, W. Skomorowski, F. Pawłowski, R. Moszynski, and Z. Idziaszek, *Phys. Rev. A* **83**, 032723 (2011).
- [51] F. H. Hall, M. Aymar, M. Raoult, O. Dulieu, and S. Willitsch, *Molecular Physics* **111**, 1683 (2013).
- [52] W. Müller and W. Meyer, *J. Chem. Phys.* **80**, 3311 (1984).

- [53] W. Müller, J. Flesch, and W. Meyer, *J. Chem. Phys.* **80**, 3297 (1984).
- [54] M. Foucrault, P. Millié, and J. Daudey, *J. Chem. Phys.* **96**, 1257 (1992).
- [55] M. Aymar and O. Dulieu, *J. Chem. Phys.* **122**, 204302 (2005).
- [56] M. Aymar and O. Dulieu, *Mol. Phys.* **105**, 1733 (2007).
- [57] A. R. Allouche and M. Aubert-Frécon, *J. Chem. Phys.* **136**, 114302 (2012).
- [58] J. Deiglmayr, A. Grochola, M. Repp, O. Dulieu, R. Wester, and M. Weidemüller, *Phys. Rev. A* **82**, 032503 (2010).
- [59] M. Aymar, J. Deiglmayr, and O. Dulieu, *Can. J. Phys.* **87**, 5443 (2009).
- [60] A. Kruzins, I. Klinkare, O. Nikolayeva, M. Tamanis, R. Ferber, E. A. Pazyuk, and A. V. Stolyarov, *Phys. Rev. A* **81**, 042509 (2010).
- [61] I. S. Lim, H. Stoll, and P. Schwerdtfeger, *J. Chem. Phys.* **124**, 034107 (2006).
- [62] I. Lim, P. Schwerdtfeger, B. Metz, and H. Stoll, *J. Chem. Phys.*, 104103 (2005).
- [63] P. J. Knowles, C. Hampel, and H. J. Werner, *J. Chem. Phys.* **99**, 5219 (1993).
- [64] H.-J. Werner, P. J. Knowles, G. Knizia, F. R. Manby, M. Schütz, *et al.*, “MOLPRO, version 2012.1: A package of ab initio programs,” (2012), see <http://www.molpro.net>.
- [65] J. F. Stanton and R. J. Bartlett, *J. Chem. Phys.* **98**, 7029 (1993).
- [66] A. I. Krylov, *Ann. Rev. Phys. Chem.* **59**, 433 (2008).
- [67] J. Stanton, J. Gauss, M. Harding, P. Szalay, *et al.*, “Cfour, a quantum chemical program package, <http://www.cfour.de>,”.
- [68] T. Helgaker, W. Klopper, H. Koch, and J. Noga, *J. Chem. Phys.* **106**, 9639 (1997).
- [69] W. Skomorowski, R. Moszynski, and C. P. Koch, *Phys. Rev. A* **85**, 043414 (2012).
- [70] D. Pavolini, T. Gustavsson, F. Spiegelmann, and J.-P. Daudey, *J. Phys. B* **22**, 1721 (1989).
- [71] G.-H. Jeung, *J. Mol. Spectrosc.* **182**, 113 (1997).
- [72] P. S. Żuchowski, M. Kosicki, M. Kodrycka, and P. Soldán, *Phys. Rev. A* **87**, 022706 (2013).
- [73] B. Friedrich and D. Herschbach, *Phys. Rev. Lett.* **74**, 4623 (1995).
- [74] M. Tomza, W. Skomorowski, M. Musiał, R. González-Frez, C. P. Koch, and R. Moszynski, *Molecular Physics* **111**, 1781 (2013).
- [75] R. González-Férez and C. P. Koch, *Phys. Rev. A* **86**, 063420 (2012).
- [76] M. Theis, G. Thalhammer, K. Winkler, M. Hellwig, G. Ruff, R. Grimm, and J. Hecker Denschlag, *Phys. Rev. Lett.* **93**, 123001 (2004).
- [77] R. Ciuryło, E. Tiesinga, and P. S. Julienne, *Phys. Rev. A* **71**, 030701 (2005).
- [78] S. Blatt, T. L. Nicholson, B. J. Bloom, J. R. Williams, J. W. Thomsen, P. S. Julienne, and J. Ye, *Phys. Rev. Lett.* **107**, 073202 (2011).
- [79] B. Jeziorski, M. Bulski, and L. Piela, *Int. J. Quantum Chem.* **10**, 281 (1976).
- [80] J. Jiang, Y. J. Cheng, and J. Mitroy, *J. Phys. B* **46**, 125004 (2013).
- [81] O. Docenko, M. Tamanis, R. Ferber, T. Bergeman, S. Kotochigova, A. V. Stolyarov, A. de Faria Nogueira, and C. E. Fellows, *Phys. Rev. A* **81**, 042511 (2010).
- [82] M. Tomza, F. Pawłowski, M. Jeziorska, C. P. Koch, and R. Moszynski, *Phys. Chem. Chem. Phys.* **13**, 18893 (2011).
- [83] M. Tomza, M. H. Goerz, M. Musiał, R. Moszynski, and C. P. Koch, *Phys. Rev. A* **86**, 043424 (2012).
- [84] W. Skomorowski, F. Pawłowski, C. P. Koch, and R. Moszynski, *J. Chem. Phys.* **136**, 194306 (2012).
- [85] C. Amiot, O. Dulieu, and J. Vergès, *Phys. Rev. Lett.* **83**, 2316 (1999).
- [86] M. Przybytek and B. Jeziorski, *J. Chem. Phys.* **123**, 134315 (2005).



